UWB Communication Characteristics for Different Distribution of People and Various Materials of Walls

Min-Hui Ho, Shu-Han Liao and Chien-Ching Chiu*

Department of Electrical Engineering, Tamkang University, Tamsui, Taiwan 251, R.O.C.

Abstract

A comparison of UWB communication characteristics for different distribution of people and various materials of walls in real environments is investigated. The impulse responses of these cases are computed by applying shooting and bouncing ray/image (SBR/Image) techniques and inverse Fourier transform. The frequency dependence utilized in the structure on the indoor channel is accounted for in the channel calculation. By using the impulse response of these multi-path channels, the mean excess delay, root mean square (RMS) delay spread, the number of multi-path arrivals within 10 dB of the peak multi-path arrival (NP10dB), and the number of paths required to meet the 85% energy capture threshold (NP (85%)) for these different distribution of people and various materials of walls have been obtained. The bit error rate (BER) performance for UWB indoor communication is calculated. The outage probability for binary antipodal-pulse amplitude modulation (B-PAM) system has been presented. Numerical results have shown that the multi-path effect by people is an important factor for BER performance. Some different distribution of people and various materials of walls have been very carefully investigated. Finally, it is worth noting that in these cases the present work provides not only comparative information but also quantitative information on the performance reduction.

Key Words: UWB, Multi-Path, Bit Error Rate, Outage Probability

1. Introduction

UWB technology has received significant interests, particularly after the Federal Communications Commission (FCC)'s Report and Order in 2002 for unlicensed uses of UWB devices within the 3.1–10.6-GHz frequency band [1]. The UWB technology has been the subject of extensive research in recent years due to its potential applications and unique capabilities. The wireless applications primarily focus on its high data rates (> 100 Mb/s) and high bandwidth for indoor short distance operation (< 10 m) applications. All wireless systems must be able to deal with the challenges of operating over a multi-path propagation channel, where objects in the environment can cause multiple reflections to arrive at the receiver. BER degradation is caused by inter-symbol interference (ISI) due to a multi-path propagation made up of radio wave reflections by walls, floor, ceiling and fixtures. Generally, 100 Mbps transmission was actually confirmed to be available for an allowable BER of 10^{-6} [2–4].

The analysis and design of an UWB communication system require an accurate channel model to determine the maximum achievable data rate, to design efficient modulation schemes, and to study associated signal-processing algorithms [5]. Besides, a prior knowledge of the characteristics of the channel is necessary for understanding how is the signal affected in the environment. Therefore, many techniques of channel calculation have been developed in recent years. Especially, using Ray-

*Corresponding author. E-mail: chiu@ee.tku.edu.tw

Tracing method to obtain impulse response is extensively applied [6–8].

The dielectric constant and the conductivity of the materials changes with frequency in the UWB. However, most papers are dealt with the same dielectric constant and conductivity of the materials for the UWB. In particular, the effect of people on the indoor channel modeling requires careful examinations before an actual implementation of UWB systems can be undertaken. Reference [9] proposes a deterministic propagation model to analyze the channel capacity of a narrowband 2.45-GHz 8 × 8 MIMO system within a small room for different distribution of people. However, to the best of our knowledge, there is no paper dealing with the effect of people on the indoor channel for the UWB communication system.

In this paper, a comparison of UWB communication characteristics for different distribution of people and various materials of walls in real environments is investigated. The effects of different materials of walls with wall board, concrete, plywood, brick, limestone and iron on the UWB communication characteristics are presented. The different values of dielectric constant and conductivity of materials and people for different frequency are carefully considered in channel calculation. Results of this research provide valuable insights into the RMS delay spread and BER performance in the UWB communication system. In section 2, a channel modeling and system description is presented. In section 3, we show the numerical results. Finally, the conclusion is drawn in section 4.

2. Channel Modeling and System Description

2.1 Channel Modeling

The following two steps are used to calculate the multi-path radio channel.

(1) Frequency responses for sinusoidal waves by SBR/Image techniques

The SBR/Image method can deal with high frequency radio wave propagation in the complex indoor environments [10,11]. It conceptually assumes that many triangular ray tubes are shot from the transmitting antenna (TX), and each ray tube, bouncing and penetrating in the environments is traced in the indoor multi-path channel. If the receiving antenna (RX) is within a ray tube, the ray tube will have contributions to the received field at the RX, and the corresponding equivalent source (image) can be determined. By summing all contributions of these images, we can obtain the total received field at the RX. In real environment, external noise in the channel propagation has been considered. The depolarization yielded by multiple reflections, refraction and first order diffraction is also taken into account in our simulations. Note that the different values of dielectric constant and conductivity of materials for different frequency are carefully considered in channel modeling.

Using ray-tracing techniques to predict channel characteristic is effective and fast [10–12]. Thus, a ray-tracing channel model is developed to calculate the channel matrix of UWB system. Flow chart of the ray-tracing process is shown in Figure 1. It conceptually assumes that many triangular ray tubes (not rays) are shot from a transmitter. Here the triangular ray tubes whose vertexes are on a sphere are determined by the following method. First, we construct an icosahedron which is made of 20 identical equilateral triangles. Then, each triangle of the icosahedron is tessellated into a lot of smaller equilateral triangles. Finally, these small triangles are projected on to the sphere and each ray tube whose vertexes are determined by the small equilateral triangle is constructed.

For each ray tube bouncing and penetrating in the environments, we check whether reflection times and penetration times of the ray tube are larger than the numbers of maximum reflection N_{ref} and maximum penetration N_{pen}, respectively. If it does not, we check whether the receiver falls within the reflected ray tube. If it does, the contribution of the ray tube to the receiver can be attributed to an equivalent source (i.e. image source). In other words, a specular ray going to receiver exists in this tube and this ray can be thought as launched from an image source. Moreover, the field diffracted from illuminated wedges of the objects in the environment is calculated by uniform theory of diffraction (UTD) [13]. Note that only first diffraction is considered in this paper, because the contribution of second diffraction is very small in the analysis.

By using these images and received fields, the channel frequency response can be obtained as following

$$H(f) = \sum_{p=1}^{N_p} a_p(f) e^{j\theta_p(f)} \tag{1}$$

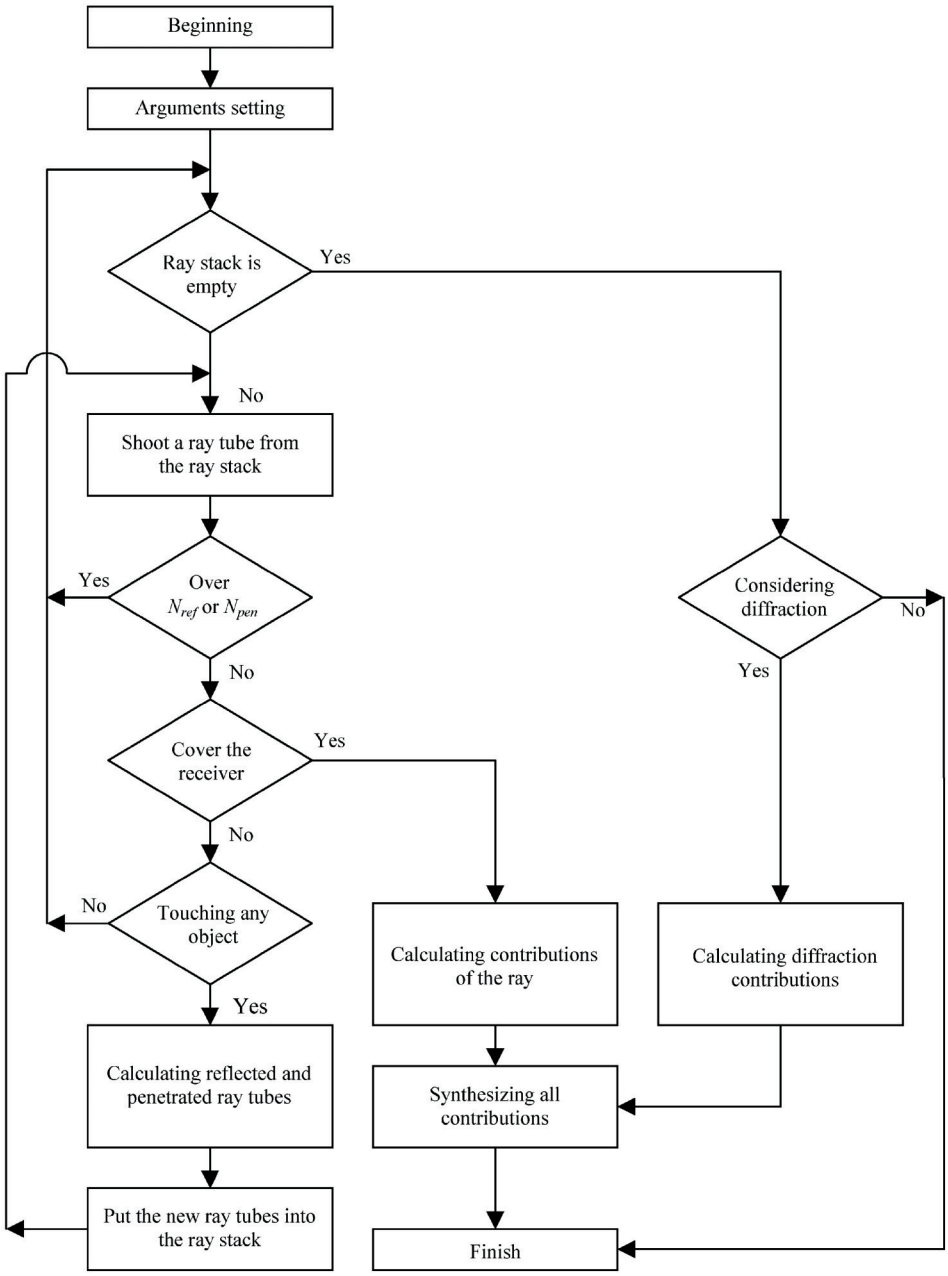

Figure 1. Flow chart of the ray-tracing process.

where p is the path index, N_p is the number of paths, f is the frequency of sinusoidal wave, $\theta_p(f)$ is the pth phase shift and $a_p(f)$ is the pth receiving magnitude. Note that the channel frequency response of UWB systems can be calculated by Eq. (1) in the frequency range of UWB for both desired signal and interference signal.

(2) Inverse fast fourier transform (IFFT) and hermitian processing

The frequency responses are transformed to the time domain by using the inverse Fourier transform with the Hermitian signal processing [14]. By using the Hermitian processing, the pass-band signal is obtained with zero padding from the lowest frequency down to direct current (DC), taking the conjugate of the signal, and reflecting it to the negative frequencies. The result is then transformed to the time domain using IFFT [15]. Since the signal spectrum is symmetric around DC. The resulting doubled-side spectrum corresponds to a real signal in the time domain. The impulse response of the channel

can be written as follows [16]:

$$h_b(t) = \sum_{n=1}^{N} a_n \, \delta(t - \tau_n) \tag{2}$$

where N is the number of paths observed at time. $\delta(\,)$ is the Dirac delta function. a_n and τ_n are the channel gain and time delay for the n-th path respectively.

2.2 System Block Diagram

The transmitted UWB pulse stream is:

$$x(t) = \sqrt{E_{tx}} \sum_{n=0}^{\infty} p(t - nT_d) \, d_n \tag{3}$$

where E_{tx} is the average transmitted energy and $p(t)$ is the transmitted waveform. T_d is the duration of the transmitting signal. $d_n \in \{\pm 1\}$ is a B-PAM symbol and is assumed to be independent identically distributed (i.i.d.). The transmitted waveform $p(t)$, as shown in Figure 2, is the second derivative Gaussian waveform with ultra-short duration T_p at the nanosecond scale. Note that T_p is the pulse duration and T_d is the duration of the transmitting signal. The value of T_d is usually much larger than that of T_p. To be radiated in an efficient way, however, a basic feature of the pulse is to have a zero dc (direct current) offset. Several pulse waveforms might be considered, provided that this condition is verified. Gaussian derivatives are suitable. Actually, the most currently adopted pulse shape is modeled as the second derivative of a Gaussian function. The second derivative Gaussian waveform $p(t)$ can be described by the following expression:

$$p(t) = \frac{d^2}{dt^2}\left(\frac{1}{\sqrt{2\pi}\sigma} e^{\frac{-t^2}{2\sigma^2}}\right) \tag{4}$$

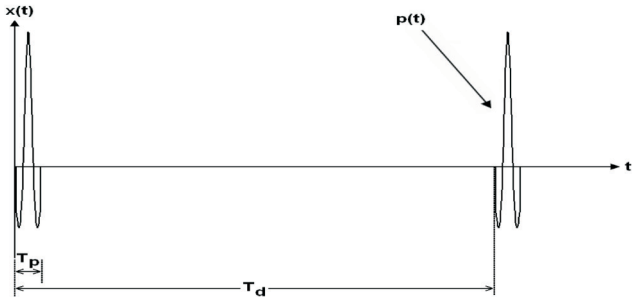

Figure 2. The diagram of transmitted waveform.

where t and σ are time and standard deviation of the Gaussian wave, respectively.

The average transmit energy symbol E_{tx} can be expressed as

$$E_{tx} = \int_0^{T_d} p^2(t)dt \tag{5}$$

Block diagram of the simulated communication system is shown in Figure 3. The received signal $r(t)$ can be expressed as follows:

$$r(t) = [x(t) \otimes h_b(t)] + n(t) \tag{6}$$

where $x(t)$ is the transmitted signal and $h_b(t)$ is the impulse response of the channel, $n(t)$ is the white Gaussian noise with zero mean and variance $N_0/2$. The correlation receiver samples the received signal at the symbol rate and correlates them with suitably delayed references given by

$$q(t) = p(t - \tau_1 - (n-1)T_d) \tag{7}$$

where τ_1 is the delay time of the first wave. The output of the correlator at $t = nT_d$ is [17,18]

$$\begin{aligned} Z(n) = & \int_{(n-1)T_d}^{nT_d} \left\{ \left[\sqrt{E_{tx}} \sum_{n=0}^{\infty} p(t - nT_d) d_n \right] \otimes h_b(t) \right\} \cdot q(t)dt \\ & + \int_{(n-1)T_d}^{nT_d} n(t)q(t)dt = V(t) + \eta(t) \end{aligned} \tag{8}$$

It can be shown that the noise components $\eta(t)$ of Eq. (8) are uncorrelated Gaussian random variable with zero mean. The variance of the output noise η is

$$\sigma^2 = \frac{N_0}{2} E_{tx} \tag{9}$$

The conditional error probability of the Nth bit is thus expressed by:

$$P_e[Z(n)|\vec{d}] = \frac{1}{2} erfc\left[\frac{V(n)}{\sqrt{2}\sigma} \cdot (d_N)\right] \tag{10}$$

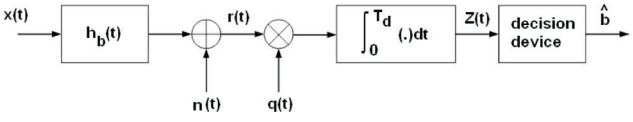

Figure 3. Block diagram of the simulated communication system.

where $erfc(x) = \frac{2}{\sqrt{\pi}} \int_x^{\infty} e^{-y^2} dy$ is complementary error function and $\{\vec{d}\} = \{d_0, d_1, ..., d_N\}$ is the binary sequence.

Finally, the average BER for B-PAM IR UWB system can be expressed as

$$BER = \sum_{n=1}^{N} P(\vec{d}) \cdot \frac{1}{2} erfc\left[\frac{V(n)}{\sqrt{2}\sigma} \cdot (d_N)\right] \quad (11)$$

where $P(\vec{d})$ is the occurring probability of the binary sequence $\vec{d}$.

3. Numerical Results

The channel characteristics for different distribution of people and various materials of walls in the indoor environments are investigated. Since the dielectric permittivity and the loss tangent of the materials changes with frequency, the different values of dielectric constant and loss tangent of materials for different frequency are carefully considered in channel calculation. For example, the relative permittivity and conductivity of human muscle is shown in Table 1 [19]. The relative permittivity and conductivity of the other different materials can be refered in [19–21]. Figure 4 is the top view of indoor environment with dimensions of 10 m (Length) × 10 m (Width) × 4.5 m (Height).

Table 1. The relative permittivity and conductivity of human muscle

Human Muscle		
Frequency (GHz)	Relative Permittivity	Conductivity (s/m)
3.0	52.058	2.1668
3.5	51.397	2.5838
4.0	50.736	3.0425
4.5	50.075	3.5429
5.0	49.414	4.0417
5.5	48.753	4.6672
6.0	48.092	5.251
6.5	47.431	5.8756
7.0	46.770	6.5004
7.5	46.109	7.1676
8.0	45.448	7.8248
8.5	44.787	8.5004
9.0	44.126	9.251
9.5	43.465	9.9166
10.0	42.804	10.6672

There are four different distribution of people and six various materials of walls considered in the simulation. Four different numbers of people with 0, 4, 12 and 36 are simulated. Materials of walls with the wall board, concrete, plywood, brick, limestone and iron are presented. 0.2 m-thick floors and ceilings of the concrete are used for these cases. Note that the conductivity and dielectric constant of materials will change with the frequency in the UWB channel. As a result, different frequencies of the same materials will have different propagation characteristics. Therefore, the frequency dependence of the dielectric and conductivity of materials is used in the channel simulation.

The parameter T_p and T_d of the second derivative Gaussian waveform $p(t)$ in the Figure 2 are set to be 0.5 ns and 10 ns respectively. The transmitting and receiving antenna are modeled as a UWB antenna with simple omni-directional radiation pattern and vertically polarized. The transmitting antenna is located at Tx (5, 5, 4) m with the fixed height of 4 m is located in the center of the indoor environment, as shown in Figure 3. There are 361 receiving points for indoor environment. The locations of receiving antennas are distributed uniformly with a fixed height of 1 m. The distance between two adjacent

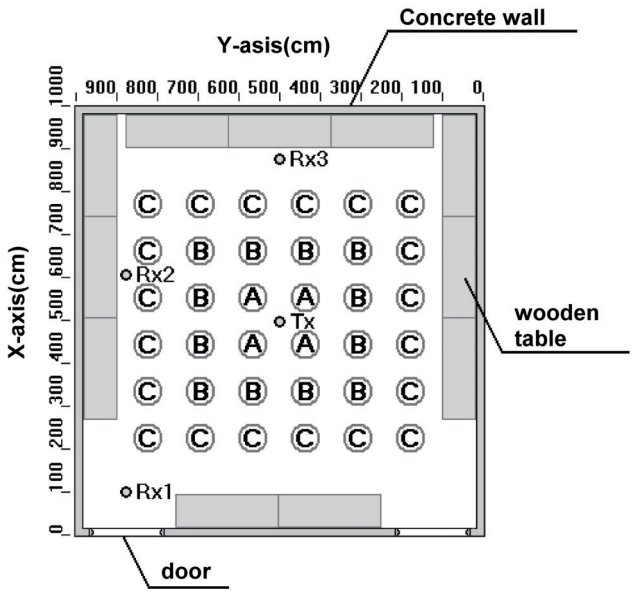

Figure 4. Top view of the indoor environment with dimensions of 10 m (Length) × 10 m (Width) × 4.5 m (Height). Tx denotes the transmitter. R × 1, R × 2 and R × 3 are the receivers in three different locations. Marks A, B and C are the positions of the people.

receiving points is 0.5 m. Meanwhile, the receiver antenna located at R × 1 (1, 1, 1) m, R × 2 (1, 6, 1) m and R × 3 (5, 9, 1) m are also plotted in Figure 4 for further discussion. The maximum number of bounces is set to be seven and the first order diffraction is also considered in the simulation.

3.1 Different Distribution of People

In the Figure 3, there are four people in the position marked A where each A represents one person. Similarly, there are twelve people on the position marked B. Finally, there are thirty-six people on the position A, B and C.

Figure 5 shows the cumulative distribution function of RMS delay spreads for different distribution of people. It is seen that the RMS delay spread value for 36 people is most serious due to the multi-path effect caused by people.

The BER versus signal-to-noise rate (SNR) for receivers at R × 2 is plotted in Figure 6. Here SNR is defined as the ratio of the average power to the noise power at the front end of the receiver. For a BER requirement of 10^{-6}, the SNR value for 36 people is larger about 4 dB than that without people. In Figure 6, it can be observed that the distributions tend to converge if the number of people is large.

By using the impulse responses of these multi-path channels, the bit error rate (BER) performance for binary pulse amplitude modulation (BPAM) impulse radio UWB communication system are calculated. Based on the BER performance, the outage probability for given 361 receiving locations of the transceiver can be computed. Outage probability statistics characteristic takes into account over all Rx location. At 100M bps transmission rate and for a BER < 10^{-6}, the outage probability versus SNR are calculated, as shown in Figure 7. It is seen that the outage probabilities at SNR = 16 dB are about 20% and 2% for the 36 people and without people respectively. It is clear that the BER performance without people is better due to the less severe multi-path effect.

Table 2 shows channel characteristics for different distribution of people. The number of people with 0, 4, 12 and 36 are considered. There are four parameters, including RMS delay spread, Mean excess delay, NP10dB and NP (85%). The RMS delay spread is the effective duration of the channel impulse response. The mean excess delay is the first moment of the channel impulse response [22]. The NP10dB is the number of multi-path arrivals

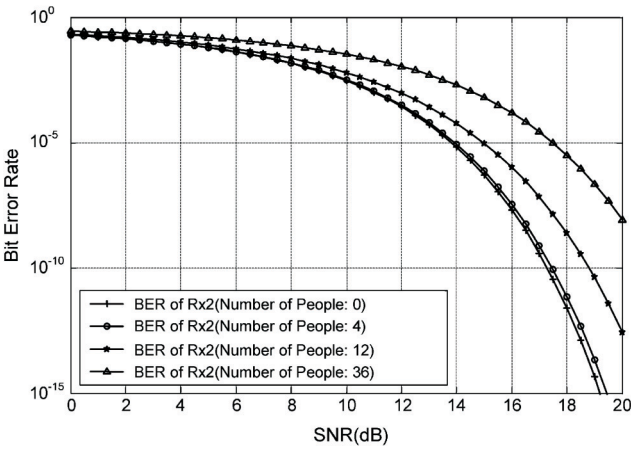

Figure 6. BER versus SNR for the different distribution of people.

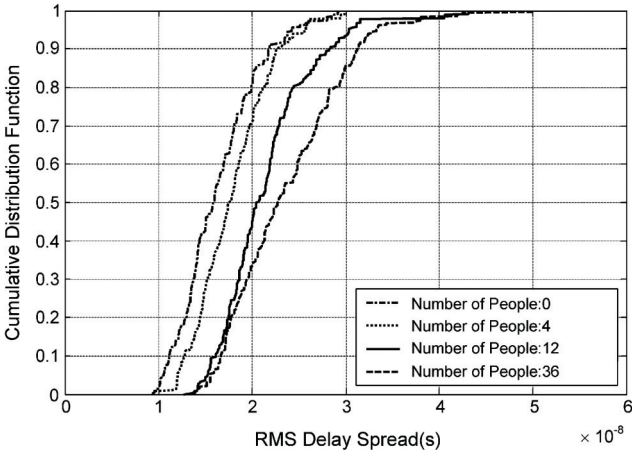

Figure 5. Cumulative distribution of RMS delay spreads for the different distribution of people.

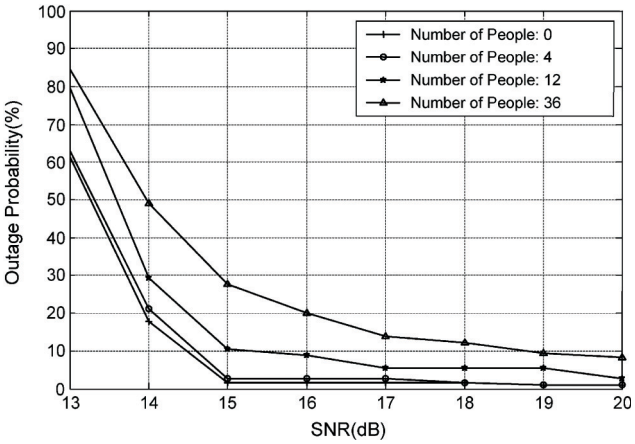

Figure 7. Outage probability versus SNR for different distribution of people.

Table 2. Parameters of multi-path channels for different distribution of people

	RMS delay spread (τ_{rms}) (ns)		Mean excess delay ($\bar{\tau}$) (ns)		NP10dB	NP(85%)
Number of People	Mean	Standard deviation	Mean	Standard deviation	mean	mean
0	16.39	4.27	10.05	3.99	5.12	31.99
4	17.91	4.04	11.02	4.95	5.14	34.72
12	21.54	5.18	14.91	9.33	6.69	52.8
36	23.68	6.14	20.19	13.21	8.23	77.82

that are within 10 dB of the peak multi-path arrival, and the NP (85%) is the number of paths required to meet the 85% energy capture threshold.

It is found that the values of RMS delay spread, Mean excess delay, NP (85%) and NP10dB increase as the number of people increase. The mean RMS delay spread without people is 16.39 ns and increases about 44% to 23.68 ns for the 36 people. It is clear that the multi-path effect is severe when the number of people increases. It is also seen that the mean excess delay without people is 10.05 ns and increases about 100% to 20.19 ns for the 36 people. Similarly, NP10dB and NP (85%) also increase a lot for 36 people. This is due to the fact that people obstruct the line-of-sight (LOS) waves and cause more multi-path effect. Note that the height of people is larger than that of the receiver. As a result, the number of receiving points for non line-of-sight (NLOS) cases increases when the number of people increases.

In the Figure 8, there are four people in the position marked A where each A represents one person. Similarly, there are twelve people on the position marked B. Finally, there are thirty-six people on the position A, B and C. This is the case that the pedestrians in Figure 4 moving one step randomly.

Figure 9 shows the cumulative distribution function of RMS delay spreads for this case. It is seen that the RMS delay spread value for 36 people is most serious due to the multi-path effect caused by people.

The BER versus signal-to-noise rate (SNR) for receivers at R × 2 is plotted in Figure 10. Here SNR is defined as the ratio of the average power to the noise power at the front end of the receiver. For a BER requirement of 10^{-6}, the SNR value for 36 people is larger about 4 dB than that without people. In Figure 10, it can be observed that the distributions tend to converge if the number of people is large. It is clear that the BER performance without people is better due to the less severe multi-path effect.

Table 3 shows channel characteristics for different distribution of pedestrians moving one step. The number of people with 0, 4, 12 and 36 are considered. There are four parameters, including RMS delay spread, Mean excess delay, NP10dB and NP (85%).

It is found that the values of RMS delay spread, Mean excess delay, NP (85%) and NP10dB increase as the number of people increase. The mean RMS delay spread without people is 16.39 ns and increases about 48% to 24.40 ns for the 36 people. It is clear that the multi-path effect is severe when the number of people increases. It is also seen that the mean excess delay without people is 10.05 ns and increases about 100% to 20.31 ns for the 36 people. It is found that value of the parameters are similar by comparing the results in Table 2 and Table 3.

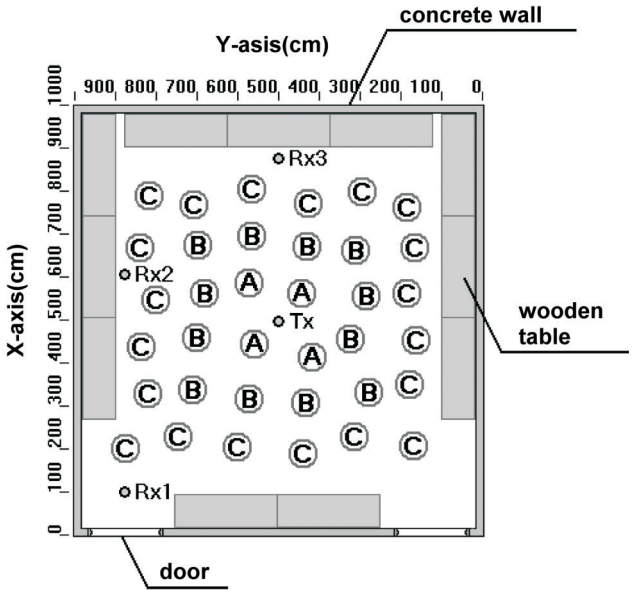

Figure 8. A top view of the simulation environment with pedestrian moving one step. Marks A, B and C are the positions of the people.

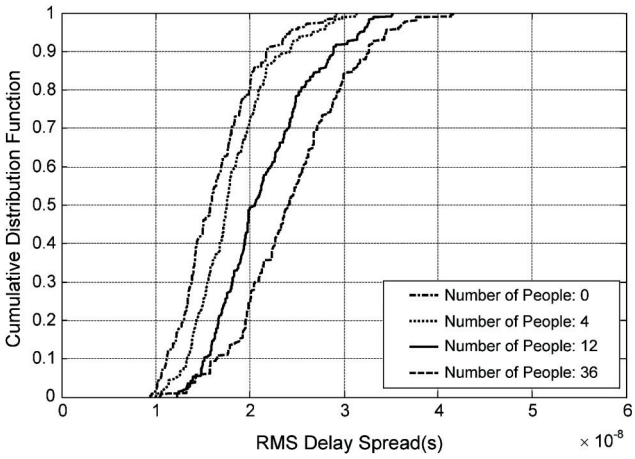

Figure 9. Cumulative distribution of RMS delay spreads for the pedestrian moving one step.

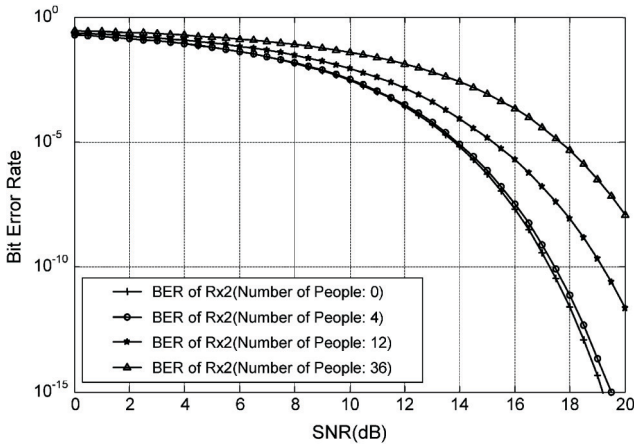

Figure 10. BER versus SNR for the pedestrian moving one step.

Table 3. Parameters of Multi-path channels for pedestrian moving one step

	RMS delay spread (τ_{rms}) (ns)		Mean excess delay ($\bar{\tau}$) (ns)		NP10dB	NP (85%)
Number of People	Mean	Standard deviation	Mean	Standard deviation	mean	mean
0	16.39	4.27	10.05	3.99	5.12	31.99
4	18.07	4.25	11.28	5.75	5.46	36.36
12	21.42	5.20	15.70	10.84	6.94	48.70
36	24.40	6.04	20.31	11.67	8.86	74.38

In the Figure 11, there are four people in the position marked A where each A represents one person. Similarly, there are twelve people on the position marked B. Finally, there are thirty-six people on the position A, B and C. This is the cases that the pedestrians moving randomly with many steps, and where applicable, pedestrian random movement. The position of transmitting and receiving antennas are the same as the previous one. UWB channel characteristics in the indoor environment with pedestrian random movement are investigated.

Figure 12 shows the cumulative distribution function of RMS delay spreads for pedestrian random movement. It is seen that the RMS delay spread value for 36 people is more serious than the other 0, 4, 12 people.

The BER versus signal-to-noise rate (SNR) for receivers at R × 2 is plotted in Figure 13. For a BER requirement of 10^{-6}, the SNR value for 36 people is larger about 4 dB than that without people. In this case, the pedestrian random movement position, directly increasing the multipath scattering present in the environment.

Table 4 shows channel characteristics for different distribution of pedestrian random movement. The number of people with 0, 4, 12 and 36 are considered. There

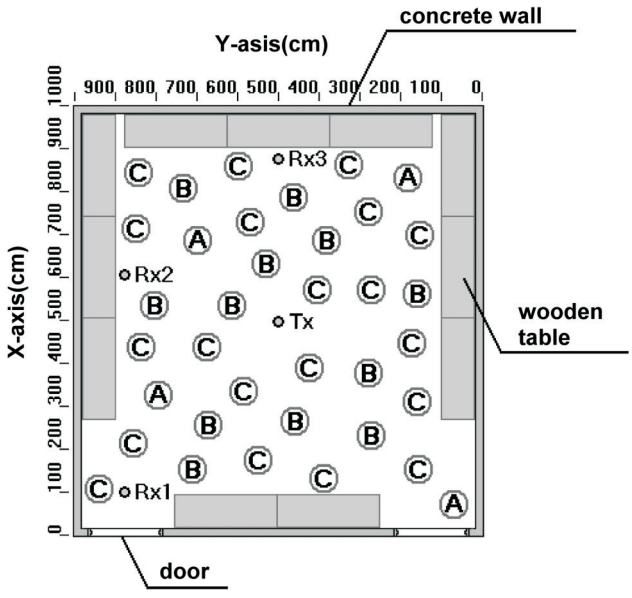

Figure 11. A top view of the simulation environment with pedestrians moving randomly with many steps. Marks A, B and C are the positions of the people.

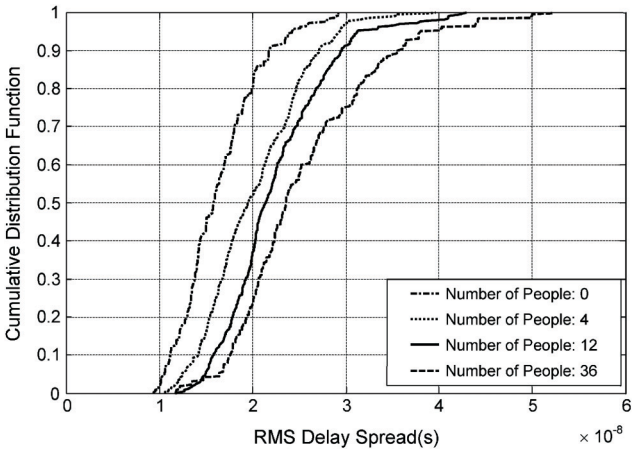

Figure 12. Cumulative distribution of RMS delay spreads for the pedestrians moving randomly with many steps.

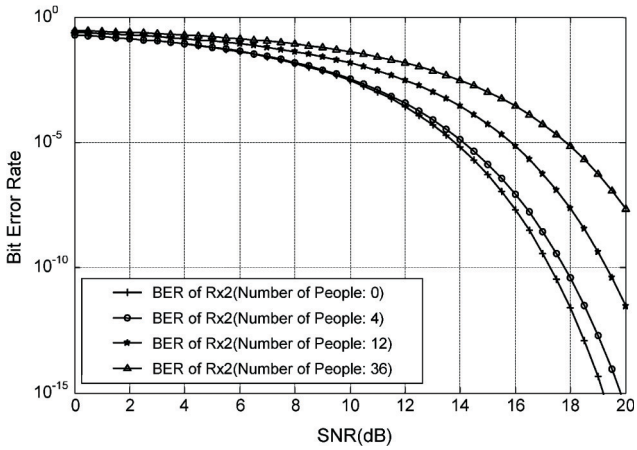

Figure 13. BER versus SNR for the pedestrians moving randomly with many steps.

Table 4. Parameters of Multi-path channels for pedestrians moving randomly with many steps

	RMS delay spread (τ_{rms}) (ns)		Mean excess delay ($\bar{\tau}$) (ns)		NP10dB	NP (85%)
Number of People	Mean	Standard deviation	Mean	Standard deviation	mean	mean
0	16.39	4.27	10.05	3.99	5.12	31.99
4	20.20	5.30	12.66	7.23	5.79	41.76
12	22.45	5.71	15.12	9.37	6.40	53.87
36	25.37	7.54	20.32	12.71	8.43	80.20

are four parameters, including RMS delay spread, Mean excess delay, NP10dB and NP (85%). It is clear that the values of RMS delay spread, Mean excess delay, NP (85%) and NP10dB for 36 people are the largest due to the strong pedestrian random movement. The mean RMS delay spread without people is 16.39 ns and increases about 55% to 25.37 ns for the 36 people. It is clear that the multi-path effect is severe when the number of people increases. Note that the value of mean excess delay for 36 people is more than twice as that for without people. It is also found that the mean excess delay increases from about 10.05 ns for the without people to about 20.32 ns for the 36 people. Similarly, NP10dB and NP (85%) also increase a lot for 36 people. It is seen that the values of the parameters change a lot by comparing the results in Table 2 and Table 4.

3.2 Various Materials of Walls

Six materials of walls with wall board, concrete, plywood, brick, limestone and iron are considered. The position of transmitting and receiving antennas are the same as the previous one except that the room is empty now. In other word, there is no people and furniture. 0.2 m-thick floors and ceilings of the concrete are used for these cases. UWB channel characteristics in the indoor environment with different materials of walls are investigated.

Figure 14 shows the cumulative distribution function of RMS delay spreads for various materials of walls. It is seen that the RMS delay spread value for wall with iron materials is more serious than the other materials of walls. The BER versus signal-to-noise rate (SNR) for receivers at R × 3 is plotted in Figure 15. For a BER requirement of 10^{-3}, the SNR value for iron wall is larger about 10 dB than that for wall board. At 100 M bps transmission rate and for a BER < 10^{-6}, the outage probability versus SNR are calculated, as shown in Figure 16. It is seen that the outage probabilities at SNR = 16 dB are about 69% and 1% for the iron wall and wall board respectively. It is clear that the BER performance for wall

board is better due to the less severe multi-path effect.

Table 5 shows channel characteristics for these six various materials of walls. There are four parameters, including RMS delay spread, Mean excess delay, NP10dB and NP (85%). It is clear that the values of RMS delay spread, Mean excess delay, NP (85%) and NP10dB for iron walls are the largest due to the strong reflection. Note that the value of RMS delay spread for iron walls is more than twice as that for wall of the other materials. It is also found that the mean excess delay increases from about 10 ns for the concrete walls to about 54 ns for the iron walls. Similarly, NP (85%) and NP10dB increase a lot for the iron walls. This situation can be explained by the fact that the multi-path effect for the iron walls is very severe due to the total reflection. Besides, it is seen that the values of RMS delay spread, Mean excess delay, NP (85%) and NP10dB for the wall board, concrete, plywood, brick and limestone are almost the same.

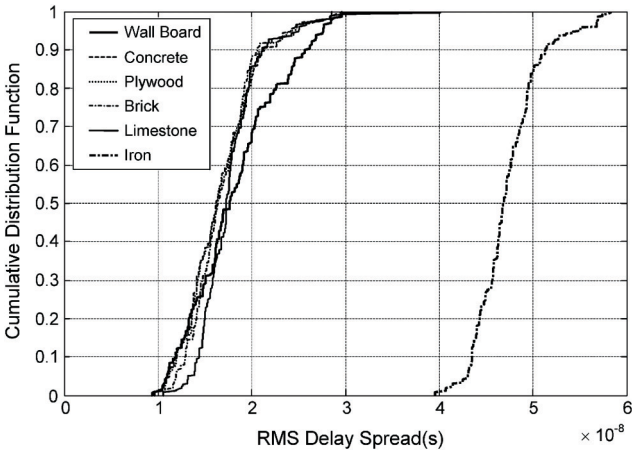

Figure 14. Cumulative distribution of RMS delay spreads for the various materials of walls.

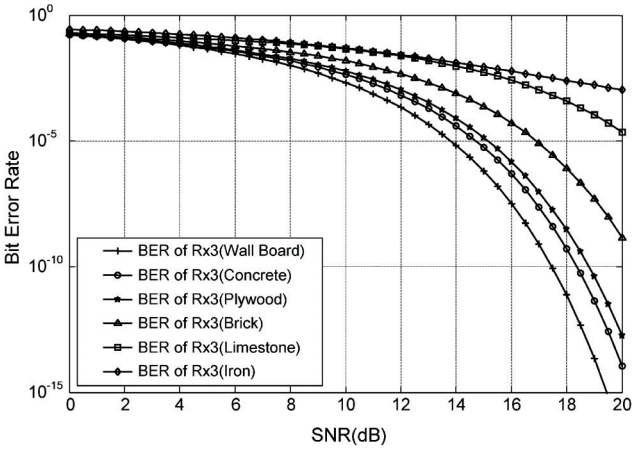

Figure 15. BER versus SNR for the various materials of walls.

4. Conclusion

A method for analyzing and calculating the channel statistical characteristics of UWB indoor communication systems has been presented. A realistic complex

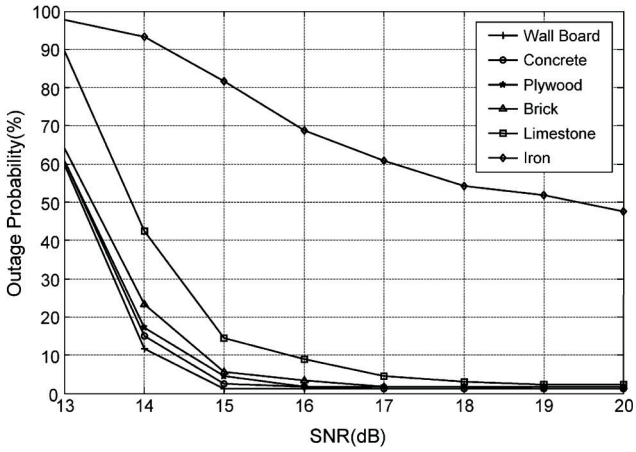

Figure 16. Outage probability versus SNR for various materials of walls.

Table 5. Parameters of multi-path channels for various materials of walls

	RMS delay spread (τ_{rms}) (ns)		Mean excess delay ($\bar{\tau}$) (ns)		NP10dB	NP(85%)
Materials of Wall	Mean	Standard deviation	Mean	Standard deviation	mean	mean
Wall Board	18.23	5.19	10.85	5.30	5.06	36.26
Concrete	16.70	4.00	10.34	4.18	5.13	34.09
Plywood	16.73	3.92	10.50	4.23	5.21	35.76
Brick	16.92	3.62	11.40	4.53	5.56	42.56
Limestone	17.66	3.26	13.00	5.04	6.22	55.29
Iron	47.31	3.49	53.86	10.07	24.26	534.38

environment is simulated in this paper. A comparison of UWB communication characteristics for different distribution of people and various materials of walls are presented. By using the impulse response of the multi-path channel, the BER for high-speed UWB indoor communication has been calculated. The frequency dependence of materials utilized in the structure on the indoor channel is accounted for in the channel simulation. i.e., the dielectric constant and conductivity of obstacles are not assumed to be frequency independent. The mean excess delay, RMS delay spread, and the number of multi-path component (NP10dB, NP(85%)) for different distribution of people and various materials of walls are computed by the SBR/Image method and inverse Fourier transform.

We analyze the fixed pedestrians and pedestrians moving one step and pedestrians moving randomly with many steps. The values of the RMS delay spread vary with different distribution of people. Numerical results show that the values of RMS delay spread, Mean excess delay, NP (85%) and NP10dB increase as the number of people increase. Moreover, the outage probabilities for 100 Mbps B-PAM and for a BER < 10^{-6} versus SNR are calculated. It is found that the outage probability for the 36 people is the largest. The performance of outage probability with people is worse than that without people in UWB environment. This is due to the multi-path effect is severe when people exist in the room.

Six materials of walls with wall board, concrete, plywood, brick, limestone and iron wall are considered. Numerical results show that iron wall in the indoor environment can result in severe multi-path and the mean RMS delay spread for the multi-path environment with iron wall effect is much larger than those for the other wall. The RMS delay spreads for iron wall are largest due to the strong multi-path effect. The BER performance for B-PAM UWB indoor communication with various materials of walls has been investigated. The impact of walls to indoor multi-path is presented and the channel statistical characteristics are analyzed. Numerical results show that outage probabilities for the UWB multi-path environment with iron wall are larger than those for the other wall. The multi-path effect is severe for the iron wall due to the total reflection. Finally, it is worth noting that in these cases the present work provides not only comparative information but also quantitative information on the performance reduction.

References

[1] Nasr, K. M., "Hybrid Channel Modelling for Ultra-Wideband Portable Multimedia Applications," *Microwaves, Antennas and Propagation, IET*, Vol. 2, pp. 229–235 (2008).

[2] Mielczarek, B., Wessman, M. O. and Svensson, A., "Performance of Coherent UWB Rake Receivers with Channel Estimators," *IEEE 58th Vehicular Technology Conference*, pp. 1880–1884 (2003).

[3] Hamalainen, M. and Iinatti, J., "Analysis of Interference on DS-UWB System in AWGN Channel," *2005 IEEE International Conference on Ultra-Wideband*, pp. 719–723 (2005).

[4] Kandukuri, S. and Boyd, S., "Optimal Power Control in Interference-Limited Fading Wireless Channels with Outage-Probability Specifications," *IEEE Transactions on Wireless Communications*, pp. 46–55 (2002).

[5] Irahhauten, Z., Nikookar, H. and Janssen, G. J. M., "An Overview of Ultra Wide Band Indoor Channel Measurements and Modeling," *IEEE Microwave and Wireless Components Letters, see also IEEE Microwave and Guided Wave Letters*, Vol. 14, pp. 386–388 (2004).

[6] Liang, G. and Bertoni, H. L., "A New Approach to 3-D Ray Tracing for Propagation Prediction in Cities," *IEEE Trans. Antennas Propagat*., Vol. 46, pp. 853–863 (1998).

[7] Zhang, Y., "Ultra-Wide Bandwidth Channel Analysis in Time Domain Using 3-D Ray Tracing," *High Frequency Postgraduate Student Colloquium of IEEE*, pp. 6–7 (2004).

[8] Woo, S., Yang, H., Park, M. and Kang, B., "Phase-Included Simulation of UWB channel," *IEICE Trans. Commum*., Vol. E88-B, pp. 1294–1297 (2005).

[9] Ziri-Castro, Karla I., Scanlon, William G., and Evans, Noel E., "Prediction of Variation in MIMO Channel Capacity for the Populated Indoor Environment Using a Radar Cross-Section-Based Pedestrian Model," *IEEE Transactions on Wireless Communications*, Vol. 4, pp. 1186–1194 (2005).

[10] Chen, S. H. and Jeng, S. K., "An SBR/Image Approach for Indoor Radio Propagation in a Corridor," *IEICE Trans. Electron*., Vol. E78-C, pp. 1058–1062 (1995).

[11] Chen, S. H. and Jeng, S. K., "SBR Image Approach for Radio Wave Propagation in Tunnels with and without Traffic," *IEEE Trans. Veh. Technol*., Vol. 45, pp. 570–578 (1996).

[12] Susana Loredo, Alberto Rodríguez-Alonso and Rafael P. Torres, "Indoor MIMO Channel modeling by Rigorous GO/UTD-Based Ray Tracing," *IEEE Trans. Veh. Technol*., Vol. 57, pp. 680–692 (2008).

[13] Balanis, Constantine A., *Advanced Engineering Electromagnetics*, John Wiley & Sons (1989).

[14] Oppermann, I., Hamalainen, M. and Iinatti, J., *UWB Theory and Applications*, John Wiley & Sons (2004).

[15] Kamen, E. W. and Heck, B. S., *Fundamentals of Signals and Systems Using the Web and Matlab*, Prentice-Hall (2000).

[16] Gabriella, M., Benedetto, D. and Giancola, G., *Understanding Ultra Wide Band Radio Fundamentals*, Prentice Hall (2004).

[17] Homier, E. A. and Scholtz, R. A., "Rapid Acquisition of Ultra-Wideband Signals in the Dense Multi-Path Channel," *IEEE Conference on Ultra Wideband Systems and Technologies*, pp. 105–109 (2002).

[18] Gargin, D. J., "A Fast and Reliable Acquisition Scheme for Detecting Ultra Wide-Band Impulse Radio Signals in the Presence of Multi-Path and Multiple Access Interference," *2004 International Workshop on Ultra Wideband Systems*, pp. 106–110 (2004).

[19] Zhao, Y., Hao, Y., Akram Alomainy and Clive Parini, "UWB On-Body Radio Channel Modeling Using Ray Theory and Subband FDTD Method," *IEEE Transactions on Microwave Theory and Techniques*, Vol. 54, pp. 1827–1835 (2006).

[20] R. Michael Buehrer, Ahmad Safaai-Jazi, William Davis and Dennis Sweeney, "Ultra-Wideband Propagation Measurements and Modeling Final Report," *DARPA NETEX Program Virginia Tech*, Chapter 3, pp. 38–216 (2004).

[21] Muqaibel, A., Safaai-Jazi, A., Bayram, A., Attiya, A. M. and Riad, S. M., "Ultrawideband Through-the-Wall Propagation," *IEE Proceedings Microwaves, Antennas and Propagation*, pp. 581–588 (2005).

[22] Rappaport, T. S., *Wireless Communications: Principles and Practice*, Prentice Hall PTR, Upper Saddle River, NJ, USA, 2nd edition (2002).

Manuscript Received: Dec. 11, 2008
Accepted: Sep. 18, 2009